Melting in Semiconductor Nanocrystals

A. N. Goldstein, C. M. Echer, A. P. Alivisatos*

New physics occurs in semiconductors when one or more dimensions of the crystal are reduced to a size comparable to bulk electron delocalization lengths (tens to hundreds of angstroms). The properties of "quantum dots" or semiconductor nanocrystals are now being studied, as techniques to fabricate the crystallites are developed. Temperature-dependent electron diffraction studies on nanocrystals of CdS show a large depression in the melting temperature with decreasing size, as a larger fraction of the total number of atoms is on the surface. Thermal stability may play a role in determining the uses of semiconductor nanocrystals.

In materials physics and chemistry the preparation of submicrometer-sized, artificially engineered semiconductor structures with new properties is a major goal. The electronic and optical properties of "quantum dots" or semiconductor crystallites that are small in comparison to bulk electron delocalization lengths (10 to 100 Å) are the subject of extensive investigations (*1–4*). Comparably sized crystallites of metals, inert gases, and molecular crystals all melt at temperatures well below the bulk melting point (*5–17*). The bonding in semiconductors, unlike that in these classes of materials, is highly directional and covalent. It is thus of interest from both theoretical and practical points of view to determine the melting temperature of semiconductor nanocrystals. In this report we demonstrate a large depression in melting temperature as size decreases for nanocrystals of a semiconductor. We find a decrease in melting temperature in clusters of the direct band gap semiconductor CdS, comparable to the depression observed in gold clusters, and as large as 1000 K for the smallest crystallites studied. Thermodynamic models based on differences in surface tension between the liquid and solid can be applied to this system, even though the bonding is highly directional.

A large variety of approaches to the preparation of semiconductor nanocrystals is currently under development, including electron beam etching of epitaxial layers, precipitation in glasses, and colloidal synthesis. In the colloidal method, precipitation in a fluid occurs in the presence of a stabilizer that binds to the growing crystal, preventing further growth or agglomeration. Particles prepared in this way can be isolated as a powder, redissolved, and evaporated or chemically attached to a substrate. Because of the flexibility in controlling the nanocrystal environment, these are the systems we have chosen to study here. Many different semiconductors can be prepared by colloidal methods, but among these CdS remains the prototypical system.

Spherical CdS nanocrystals are prepared by arrested precipitation reactions with the particle surfaces being terminated with either thiophenol (*18*) or mercaptoacetic acid (*19*). The thiophenol-capped particles are prepared in inverse micelles. The colloids are isolated as a dry powder, which is redissolvable in pyridine. Water-soluble particles are synthesized by the combination of $CdCl_2$ and mercaptoacetic acid to give an extended complex that is destabilized by a change in pH, followed by addition of Na_2S. The standard deviation in size for a given sample is ±7% in diameter, as determined by x-ray powder diffraction (XRD), transmission electron microscopy (TEM), and ultraviolet-visible spectrometry.

In this work we present a TEM study of melting temperature (T_m) for CdS nanocrystals ranging in diameter from 24 to 76 Å; T_m is defined as the temperature corresponding to the disappearance of electron diffraction peaks associated with the solid in selected area diffraction (SAD) patterns. The electron diffraction experiments were conducted so as to minimize spurious beam heating. Experiments used a 0.2-μm^2 field of particles dispersed on a thin amorphous carbon film in a JEOL 200 analytical microscope operating at 200 kV with condenser and objective lens currents controlled to ±0.002 A. Beam current was maintained at 8 μA above the dark current, well below fluxes commonly required to effect beam-induced transformations (*20*). Under these conditions the calculated beam heating of the sample is no more than 0.25 K, within the kinematic scattering approximation (*21, 22*). Camera constants were calibrated with room-temperature diffraction patterns of samples with XRD-determined *d*-spacings (interatomic spacings). A calibrated thermocouple monitored the temperature of the furnace. We checked the thermocouple calibration by examining the reversible phase transition of α-quartz to β-quartz, which occurs at 846 K; this transition was observed repeatedly in our hot stage within ±2 K of this temperature, confirming that electron beam heating is of little consequence.

The experimental procedure consisted of heating to at least one-third T_m and incrementally cooling before the melting cycle to further anneal the particles. The substrates were resistively heated in 25 K steps with a tantalum furnace hot stage to 50 K beyond T_m and cooled stepwise. Concurrent bright- and dark-field observations of the particles were made. The (111) diffraction ring was used in image formation for dark-field observations. We measured T_m in two different ways with identical results. In the first, the disappearance of a particle in a dark-field image, indicating a change in *d*-spacing associated with the phase transition, provided the T_m of an individual crystallite. In the second method, the intensity of the diffraction from an ensemble of particles was integrated. The ring diffraction patterns obtained at each temperature were digitized with a 2048-channel linear array charge-coupled device and radially integrated through the pattern center over a 5° arc. High-resolution TEM images were obtained before and after melting studies to assess changes in lattice structure and particle morphology by means of a JEOL 200CX with 2 Å spatial resolution at 200 kV. The identical nanocrystals were placed on a thin polycrystalline beryllium oxide film and heated to 673 K. Diffraction patterns were collected before and after heating to determine the effect of surface capping molecules on the lattice parameter of CdS.

The results of a heating cycle are shown in Fig. 1, A through F. The atomic resolution image of a single thiophenol-capped particle before heating shows spots, which are produced by columns of atoms parallel to the beam axis. When these particles are dispersed at sufficiently low densities such that there is no contact between particles, melting and recrystallization occur as demonstrated by the SAD patterns before (Fig. 1C) and after (Fig. 1F) melting from different fields on the same grid. At low density the crystallite size is unchanged, but the domain size from the Scherrer formula is in accord with the particle diameter after melting and recrystallization. Real space observations of single particles show them to be a nonwetting fluid above T_m and meandering slowly across the surface. At high particle densities the molten particles fuse to produce a thin polycrystalline film. The extended CdS formed by crystallite fusion appears to show a preferential orientation on the amorphous carbon substrate with ⟨111⟩ planes lying parallel to the substrate. Energy-dispersive spectroscopy on

A. N. Goldstein and A. P. Alivisatos, Department of Chemistry, University of California, Berkeley, and Materials Sciences Division, Lawrence Berkeley Laboratory, Berkeley, CA 94720.
C. M. Echer, National Center for Electron Microscopy, Lawrence Berkeley Laboratory, Berkeley, CA 94720.
*To whom correspondence should be addressed.

particle fields before and after melting shows that the stoichiometry of the sample is maintained upon accounting for the loss of thiol-capping moieties.

For a given size, all the electron diffraction peaks associated with the CdS nanocrystals drop rapidly above the melting temperature and completely disappear into the amorphous carbon background. This process is reversible and occurs below the bulk T_m of CdS of 1678 K. The nanocrystal electron diffraction linewidths do not change appreciably with temperature and are consistent with real space observations, which suggest that melting occurs throughout the entire particle in a narrow range of temperature. The thermal expansion of the particle lattice is not accurately determinable with present electron diffraction angular resolution. The decay of log intensity as a function of temperature shows a great deal of scatter but is linear at low temperatures (relative to T_m) implying only a weak dependence of the Debye-Waller factor on size (Fig. 2). For a given size T_m does not appear to depend on the nature of the surface-capping moiety. Temperature-programmed desorption mass spectrometry demonstrates that the thiophenol and mercaptoacetic acid desorb at 523 and 463 K, respectively, below T_m of the smallest crystallites (573 K). The organic stabilizers are therefore volatilized in the course of the annealing cycle preceding melting, and the T_m measured is that for a bare nanocrystal supported on an amorphous C substrate.

The predictions of simple thermodynamic models of melting point reduction based on the surface tension difference between the liquid and solid phases agree reasonably well with size-dependent melting of metal nanocrystals (*5, 11, 23, 24*). The use of surface tension to describe a solid particle involves the approximation that creating the surface generates forces that press radially inward from all sides, and no net forces in the plane of the surface. The application of the surface tension concept to semiconductor surfaces is therefore somewhat more problematic in this system than in the case of metals. The reconstruction of the surfaces of cleavage planes of bulk semiconductors is extremely specific, involving in-plane angular distortions as well as contractions. In nanocrystals, however, many cleavage planes are likely to be present simultaneously, and the exact surface structure is unknown. The need to quantify the large size dependence of the phase diagram in the absence of detailed knowledge of the surface bonding geometry leads us back to the concept of surface tension (*25*). We find that this approach suffices to quantify the present measurements of T_m as a function of size for CdS. As in the case of metals, the melting of the

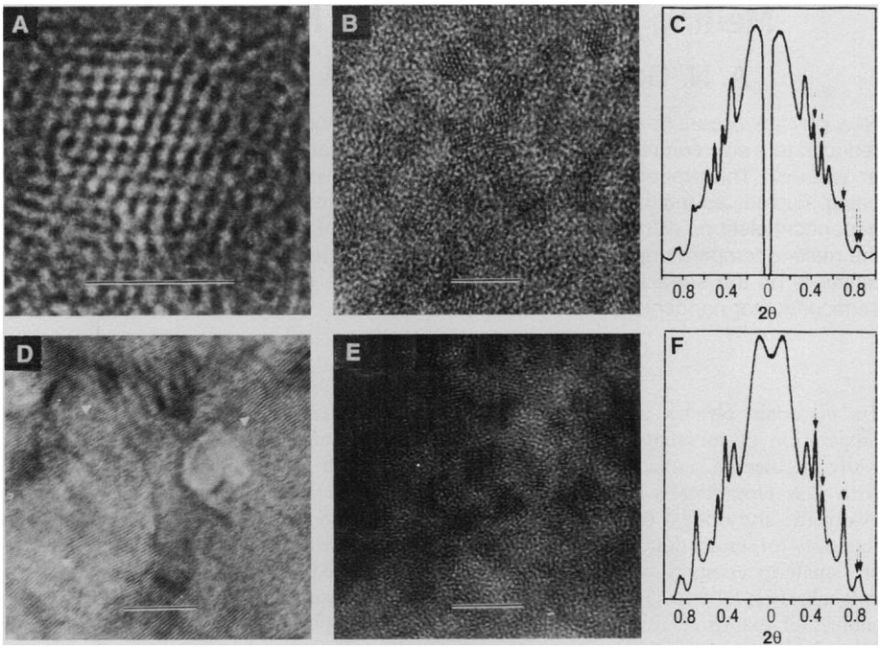

Fig. 1. The sequence of events during a melting experiment. The length marker in (A) is 30 Å; in the other panels the length marker represents 50 Å. (**A**) High-resolution micrograph of a single 30 Å CdS nanocrystal before heating. (**B**) Field of particles before heating. (**C**) The corresponding radially averaged ring diffraction pattern. (**D**) Polycrystalline thin film formed by melting and fusing nanocrystals in a region of high nanocrystal density on the grid [(111) planes are evident diagonally across the micrograph and can be seen along the directions of the white arrows]. (**E**) Field of isolated particles after a melting cycle. The shape and size are preserved from (B). (**F**) The diffraction pattern from isolated particles after melting shows increased crystallinity. The arrows in (C) and (F) denote the (111), (200), (220), (311), and (222) peaks of CdS. Peaks with no arrows above them are from the amorphous C substrate.

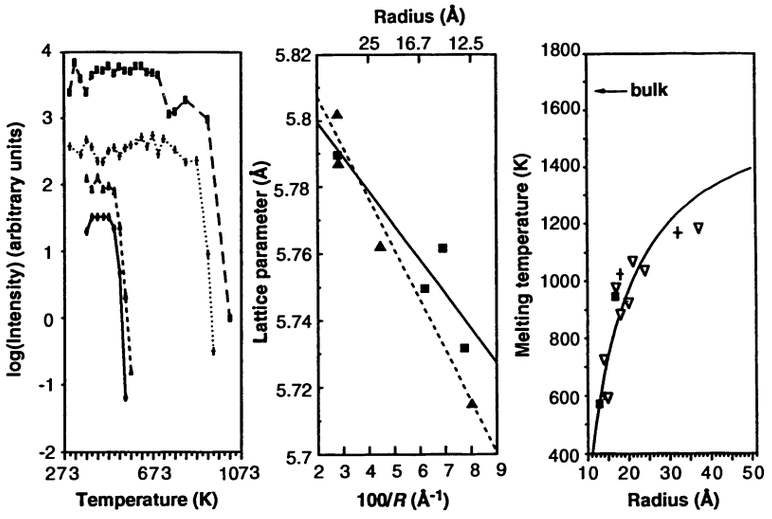

Fig. 2 (left). Logarithm of the intensity of electron diffraction from the (111) peak as a function of temperature for several sizes of CdS nanocrystals. The curves have been arbitrarily offset vertically for visual clarity. For each size, there is a sharp decrease in log intensity above the melting temperature. (◇ and solid line), 12 Å radius; (△ and short dashed line), 13 Å radius; (+ and dotted line), 16 Å radius; (■ and long dashed line), 18 Å radius. **Fig. 3 (center).** Lattice parameter of CdS nanocrystals as a function of the reciprocal particle radius, R. (▲) Points from bare nanocrystals; the dashed line for bare nanocrystals yields a surface tension of 2.50 N m^{-1}. (■) Points from mercaptoacetic acid–capped nanocrystals; the solid line fit yields a surface tension of 1.74 N m^{-1}. **Fig. 4 (right).** Size dependence of T_m for CdS nanocrystals. (■ and +) T_m derived from the disappearance of electron diffraction from an ensemble of thiophenol (or mercaptoacetic acid)–capped nanocrystals; (▽), T_m derived by observing the change in dark field of a single CdS particle. The solid curve represents a fit to Eq. 1 using γ_{sol} derived from Fig. 3.

CdS will occur when the chemical potentials of the solid and liquid phases are equal. If the assumption of a three-phase equilibrium between a spherical solid particle, a liquid particle of the same mass, and vapor is made, changes in T_m compared to that of the bulk are given by (5)

$$T_b - T_m = \frac{2T_m}{L\,\rho_{sol}\,R_{sol}}\left[\gamma_{sol} - \gamma_{liq}\left(\frac{\rho_{sol}}{\rho_{liq}}\right)^{2/3}\right] \quad (1)$$

where T_b is the bulk melting temperature, T_m is the melting temperature for a particle of radius R, L is the molar latent heat of fusion, and γ and ρ are the surface tension and density, respectively. All parameters for this equation are known or are reliably estimated, with the exception of the surface tensions. A fit of Eq. 1 to T_m as a function of reciprocal particle radius yields a difference in surface tensions $\gamma_{sol} - \gamma_{liq}$ of 0.42 N m^{-1}. Thus, if either surface tension is determined independently, both are known.

The surface tension of the solid can be obtained from the contraction of the lattice with decreasing size at room temperature (Fig. 3). The slope of this plot is related to γ by

$$\frac{\Delta a}{a} = \frac{2}{3}\frac{\gamma\kappa}{R} \quad (2)$$

where κ is the isothermal compressibility ($\kappa_{CdS} = 1.56 \times 10^{-11}$ m^2 N^{-1}). High-pressure studies have shown that the isothermal compressibility of the nanocrystals is the same as for the bulk (26). These plots yield a value of $\gamma_{sol}(111)$ for capped particles of 1.74 ± 0.11 N m^{-1}, whereas γ_{sol} for the bare nanocrystals is 2.50 N m^{-1} (Fig. 3). This compares with an experimental bulk $CdS_{(111)}$ surface tension of 0.750 N m^{-1} (27, 28) and a calculated value of 0.865 N m^{-1} (29). The fit of Eq. 1 is obtained with a value for $\gamma_{sol} - \gamma_{liq}$ of 0.42 N m^{-1} and the values of ρ_{sol} and L, which are 4830 kg m^{-3} and 50.6 kcal mol^{-1}, respectively. The density of liquid CdS is assumed to be 4200 kg m^{-3}. The large increase in surface tension for CdS nanocrystals, compared to that of the bulk, is consistent with observations in metallic systems such as Al (30), Pt, and Au (31). Surface stress coefficients for the (422) faces of Pt and Au are 4.44 and 3.19 N m^{-1}, respectively, whereas the corresponding bulk surface tensions are approximately 3.1 and 1.8 N m^{-1}. Solliard and Flueli have argued that this increase in surface tension for the nanocrystals, compared to that of the bulk, is attributable to a weak dilation of the surface (31).

The marked reduction in T_m for semiconductor nanocrystals has several important implications. First, the optimum annealing temperature for preparation of high-quality, defect-free nanocrystals can be expected to be a small fraction of the bulk annealing temperature. Second, the ability to fuse nanocrystals to form a film at relatively modest temperatures indicates that nanocrystals may provide a new low-temperature route to thin-film growth. Finally, as the dimension of active domains is reduced to the nanometer length scale, the thermal stability of the new devices may be limited. Large changes in the phase diagram as well as in the electronic properties must be considered in semiconductors of reduced dimensionality.

REFERENCES AND NOTES

1. D. A. B. Miller, D. S. Chemla, S. Schmitt-Rink, in *Optical Nonlinearities and Instabilities in Semiconductors*, H. Haug, Ed. (Academic Press, Orlando, FL, 1988), p. 325.
2. M. L. Steigerwald and L. E. Brus, *Annu. Rev. Mater. Sci.* **19**, 471 (1989).
3. G. D. Stucky and J. E. Mac Dougall, *Science* **247**, 669 (1990).
4. A. Henglein, *Top. Curr. Chem.* **143**, 113 (1988).
5. Ph. Buffat and J.-P. Borel, *Phys. Rev. A* **13**, 2287 (1976).
6. S. J. Peppiat and J. R. Sambles, *Proc. R. Soc. London Ser. A* **345**, 387 (1975).
7. M. Y. Hahn and R. L. Whetten, *Phys. Rev. Lett.* **61**, 1190 (1988).
8. P. Sheng *et al.*, *J. Phys. C* **14**, L565 (1981).
9. C. Solliard, *Surf. Sci.* **106**, 58 (1981).
10. C. J. Coombes, *J. Phys. F* **2**, 441 (1972).
11. P. Pawlow, *Z. Phys.* **66**, 549 (1909).
12. C. L. Briant and J. J. Burton, *J. Chem. Phys.* **63**, 2045 (1975).
13. R. S. Berry, J. Jellinek, G. Natanson, *Phys. Rev. A* **30**, 919 (1984).
14. W. D. Kristensen, E. J. Jensen, R. M. Cotterill, *J. Chem. Phys.* **11**, 4161 (1974).
15. J. D. Honeycutt and H. C. Andersen, *ibid.* **91**, 4950 (1987).
16. K.-J. Hanzen, *Z. Phys.* **157**, 523 (1960).
17. M. Hasegawa, K. Hoshino, M. Watabe, *J. Phys. F* **10**, 619 (1980).
18. M. L. Steigerwald *et al.*, *J. Am. Chem. Soc.* **110**, 3046 (1988).
19. Y. Nosaka *et al.*, *Chem. Lett.* **1988**, 605 (1988); A. P. Alivisatos *et al.*, *Mater. Res. Soc. Symp. Proc.* **195**, 597 (1990); V. L. Colvin, A. N. Goldstein, A. P. Alivisatos, *J. Am. Chem. Soc.*, in press.
20. E. P. Butler and K. F. Hale, in *Dynamic Experiments in the Electron Microscope*, A. M. Glauert, Ed. (Van Nostrand, New York, 1981), vol. 9, pp. 112–119.
21. B. Gale and K. F. Hale, *Br. J. Appl. Phys.* **12**, 116 (1961).
22. J. Ling, *ibid.* **18**, 991 (1967).
23. C. R. Wronski, *ibid.*, p. 1731.
24. H. Reiss and I. B. Wilson, *J. Colloid Sci.* **3**, 551 (1948).
25. A. Zangwill, *Physics at Surfaces* (Cambridge Univ. Press, Cambridge, 1988).
26. M. Haase and A. P. Alivisatos, *Mater. Res. Soc. Symp. Proc.* **206**, 233 (1991); *J. Phys. Chem.*, in press.
27. B. F. Ormont, *Dokl. Akad. Nauk SSSR* **124**, 132 (1959).
28. S. N. Sadumkin, *Fiz. Tverd. Tela* **2**, 880 (1960).
29. B. N. Oshcherin, *Phys. Status Solidi A* **34**, K181 (1976).
30. J. Woltersdorf, A. S. Nepijko, E. Pippel, *Surf. Sci.* **106**, 64 (1981).
31. C. Solliard and M. Flueli, *ibid.* **156**, 487 (1985).

32. We thank V. Colvin for preparing the samples. We thank J. H. Turner and M. A. O'Keefe for assistance in digitizing the electron diffraction patterns obtained in this study. We also thank the National Center for Electron Microscopy for the use of their facilities. This work was supported by the Director, Office of Basic Energy Sciences, Division of Materials Sciences, of the U.S. Department of Energy under contract DEAC03-76SF00098.

13 January 1992; accepted 8 April 1992

Pressure-Induced Coordination Changes in Alkali-Germanate Melts: An in Situ Spectroscopic Investigation

Daniel L. Farber and Quentin Williams

The structure of liquid $Na_2Ge_2O_5{\cdot}H_2O$, a silicate melt analog, has been studied with Raman spectroscopy to pressures of 2.2 gigapascals. Upon compression, a peak near ~240 wavenumbers associated with octahedral GeO_6 groups grows relative to a peak near ~500 wavenumbers associated with tetrahedral GeO_4 groups. This change corresponds to an increase in octahedral germanium in the liquid from near 0% at ambient pressures to >50% at a pressure of 2.2 gigapascals. Silicate liquids plausibly undergo similar coordination changes at depth in the Earth. Such structural changes may generate decreases in the fusion slopes of silicates at high pressures as well as neutrally buoyant magmas within the transition zone of the Earth's mantle.

Pressure-induced changes in the coordination number of silicon from four- to sixfold with respect to oxygen profoundly alter the physical and chemical properties of minerals in the deep Earth (*1*). However, comparable structural changes in silicate melts have only been inferred to occur at high pressures. Resolving the structure of melts at high pressures and temperatures requires actual experiments on pressurized, high-temperature liquids. We describe spectroscopic measurements made on a silicate-analog (germanate) liquid in situ at simultaneous high-pressure and high-temperature conditions.

Earth Sciences Board and Institute of Tectonics, University of California, Santa Cruz, CA 95064.